Editors' Suggestion

Collective Magnetic Excitations in a Photoexcited Electron-Doped Cuprate Superconductor

Daniel Jost,[1,*] Jiarui Li,[1,*] Jordyn Hales,[2] Jonathan Sobota,[1] Giacomo Merzoni,[3,4] Leonardo Martinelli,[4,§] Shuhan Ding,[2] Ke-Jun Xu,[1,5,7] Justine Schlappa,[3] Andreas Scherz,[3] Robert Carley,[3] Benjamin E. Van Kuiken,[3] Teguh C. Asmara,[3] Le Phuong Hoang,[3] Laurent Mercadier,[3] Sergii Parchenko,[3] Martin Teichmann,[3] Patrick S. Kirchmann,[1] Giacomo Ghiringhelli,[4,6] Brian Moritz,[1] Zhi-Xun Shen,[1,7,5,8] Thomas P. Devereaux,[1,9,7] Yao Wang,[2,†] and Wei-Sheng Lee[1,‡]

[1]*Stanford Institute for Materials and Energy Sciences, SLAC National Accelerator Laboratory, Menlo Park, California 94025, USA*
[2]*Department of Chemistry, Emory University, Atlanta, Georgia 30322, USA*
[3]*European XFEL, Holzkoppel 4, Schenefeld 22869, Germany*
[4]*Dipartimento di Fisica, Politecnico di Milano, piazza Leonardo da Vinci 32, I-20133 Milano, Italy*
[5]*Department of Applied Physics, Stanford University, Stanford, California 94305, USA*
[6]*CNR-SPIN, Dipartimento di Fisica, Politecnico di Milano, I-20133 Milano, Italy*
[7]*Geballe Laboratory for Advanced Materials, Stanford University, Stanford, California 94305, USA*
[8]*Department of Physics, Stanford University, Stanford, California 94305, USA*
[9]*Department of Materials Science and Engineering, Stanford University, Stanford, California 94305, USA*

(Received 25 February 2026; accepted 29 June 2026; published 26 August 2026)

Elucidating the microscopic behavior of cuprates under ultrafast photoexcitation offers critical insights into their highly correlated out-of-equilibrium states. Although quasiparticle dynamics have been investigated extensively, the behavior of collective magnetic excitations remains comparatively unexplored. Here, we use time-resolved resonant inelastic x-ray scattering at the Cu L_3-edge to track the collective magnetic excitations (paramagnons) in an optimally electron-doped cuprate driven out-of-equilibrium by a femtosecond pump laser pulse. Upon pumping, we observed an anti-Stokes signal associated with paramagnon generation, which modifies the paramagnon dispersion near the zone center, although the bandwidth remained unchanged. Moreover, the spectral weight exhibits a momentum-dependent variation across the Brillouin zone. The light-driven boost of the paramagnon population and the resulting spectral-weight transfer could provide new leverage to manipulate the properties of cuprates.

DOI: 10.1103/2h9x-8tjk

In high-T_c superconducting cuprates, antiferromagnetic (AFM) correlations and doped charge carriers form a complex and strongly intertwined many-body wave function, which can manifest distinct quantum phases by changing doping and temperature [1]. By driving charge and spin degrees of freedom via photoexcitation, the wave function could be transiently modified, affecting the electronic properties of cuprates [2] and potentially lead to a state without an equilibrium analog [3–5]. Time-resolved optical spectroscopy [6], angle-resolved photoemission spectroscopy [7], and x-ray scattering [8–12] have elucidated extensive information about the photoexcited response of electronic bands, superconducting pairs, and the lattice, as well as charge order. However, collective excitations of spin, which bears the hallmark of spin exchange interaction and information of its coupling to the charges [1], remain largely unexplored in photoexcited cuprates due to the lack of a suitable probe.

Time-resolved resonant inelastic x-ray scattering (trRIXS), which is capable of tracking collective excitations in time, energy, and momentum [13,14] can be an ideal tool. Although the advent of x-ray free-electron lasers (FEL) a decade ago has enabled trRIXS measurements [10,15–18], comprehensive high-resolution trRIXS measurements on cuprates have only recently become possible due to the availability of high-repetition-rate soft x-ray FELs and high-resolution trRIXS instruments [19].

In this Letter, we focus on the electron-doped cuprate $Nd_{2-x}Ce_xCuO_4$ (NCCO), a material whose phase diagram is characterized by a prominent antiferromagnetic phase [20,21]. The underlying AFM correlation plays a critical role in shaping the electronic structure [22] and influences the emergence of superconducting coherence in the underdoped regime [23]. At optimal doping ($x \sim 0.15$), the spin correlation length becomes short-ranged—about 20 unit

*These authors contributed equally to this work.
†Contact author: yao.wang@emory.edu
‡Contact author: leews@stanford.edu
§Present address: Physik-Institut, Universität Zürich, Winterthurerstrasse 190, CH-8057 Zürich, Switzerland.

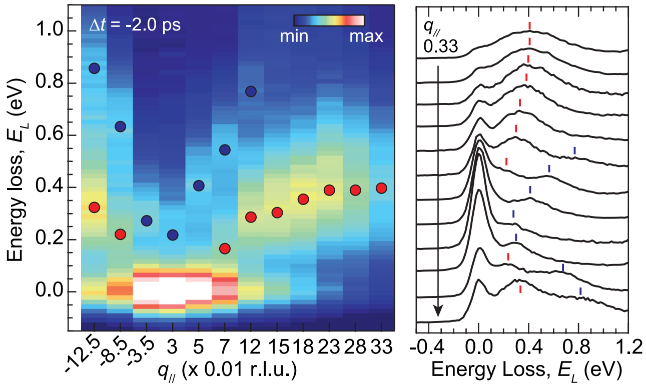

FIG. 1. Energy-momentum RIXS intensity map (left) taken before time zero (Δt = -2.0 ps). The measured momenta appear as discrete points along the horizontal axis, not on a linear value scale. The waterfall plot of RIXS spectra are shown in the right panel. The red and blue markers indicate the paramagnon and plasmon peaks, respectively.

cells [20]—yet still couples to quasiparticles at the Fermi energy, reconstructing the Fermi surface and producing a pseudogap at the "hot spot" where it intersects the AFM zone boundary [21,22,24]. Interestingly, time-resolved angle-resolved photoemission spectroscopy (tr-ARPES) has demonstrated that photoexcitation results in the filling of this pseudogap, an effect previously linked to a decrease in the spin correlation length [25]. Nevertheless, a comprehensive understanding of the underlying microscopic dynamics remains elusive, as a direct spectroscopic interrogation of collective spin excitations in the photoexcited state is still lacking.

Here, we use trRIXS to track the time evolution of magnetic excitations in electron-doped superconducting cuprate $Nd_{2-x}Ce_xCuO_4$ (NCCO) at optimal doping $x \sim 0.15$. The energy and time resolution of the trRIXS measurement were approximately 120 meV and 0.15 ps, respectively. Further details of the experiment are described in Supplemental Material [26]. Although a pump laser pulse at 800 nm (corresponding to a photon energy of ~1.55 eV) is most commonly used for photoexcitation, we instead excited the system with 400 nm laser pulses (~3.1 eV) at a fluence of $7\ \mathrm{mJ/cm^2}$, as the optical absorption is higher at this wavelength [27]. We note that in optimally doped NCCO the optical conductivity is essentially featureless above 1.0 eV [27], implying that the excitation induced by the 400 nm pump pulse is similar to that produced by the 800 nm pump pulse. In both cases, photoexcitation creates "hot" electrons, whose temporal evolution is often described phenomenologically using a multitemperature model [7,28]. Our observation of collective magnetic excitations adds the missing element—the spin degree of freedom—to the microscopic picture of photoexcited cuprates.

Figure 1 shows the RIXS intensity as a function of energy loss E_L and momentum transfer $q_\parallel$ along the Cu-O bond direction (i.e., the h direction), measured with x-ray FEL pulses before time zero, defined as the arrival time of the pump pulse at the sample. Dispersive paramagnons are evident, emanating from the zone center ($q_\parallel = 0$) toward the zone boundary ($q_\parallel = 0.5$) with a bandwidth of approximately 400 meV. In addition, another branch of rapidly dispersing charge modes, acoustic plasmons [29,30], can be resolved near the zone center. These spectra are consistent with previous static RIXS measurements using x-rays from synchrotron light sources [29–32].

To evaluate the light-driven effects, we analyzed the differential RIXS spectra ΔI, as shown in Figs. 2(a) and 2(b), obtained by subtracting the spectra at time delay $\Delta t = 0.25$ ps from those at $\Delta t = -2.0$ ps. The changes, particularly the intensity depletion highlighted in blue,

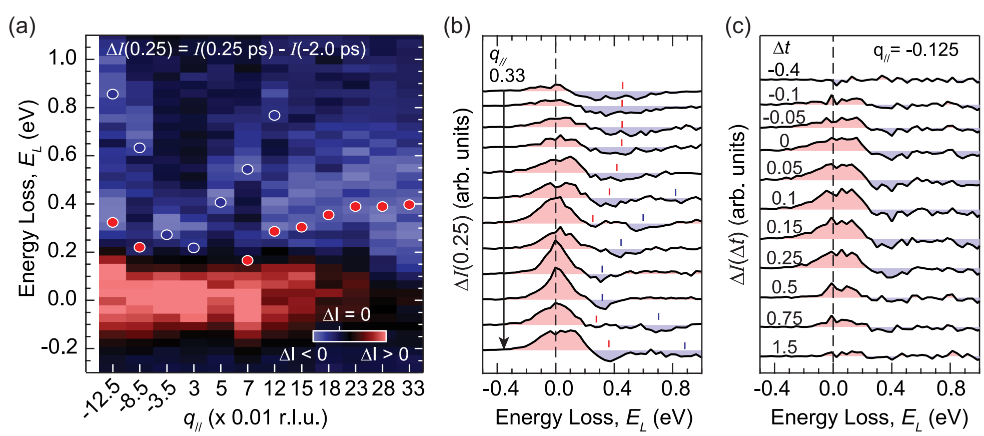

FIG. 2. (a) Differential RIXS intensity map obtained by subtracting the RIXS map taken at $\Delta t = 0.25$ ps from that taken at-2.0 ps. The measured momenta appear as discrete points along the horizontal axis, not on a linear value scale. The red and blue markers indicated the peak positions of paramagnon and plasmon, same as those shown in Fig. 1. (b) Waterfall plot of the differential RIXS spectra of panel (a). The red and blue ticks indicate the variations associated near the peaks of paramagnon and plasmon, respectively. (c) Differential spectral at $q_\parallel = -0.125$ r.l.u. taken at different Δt.

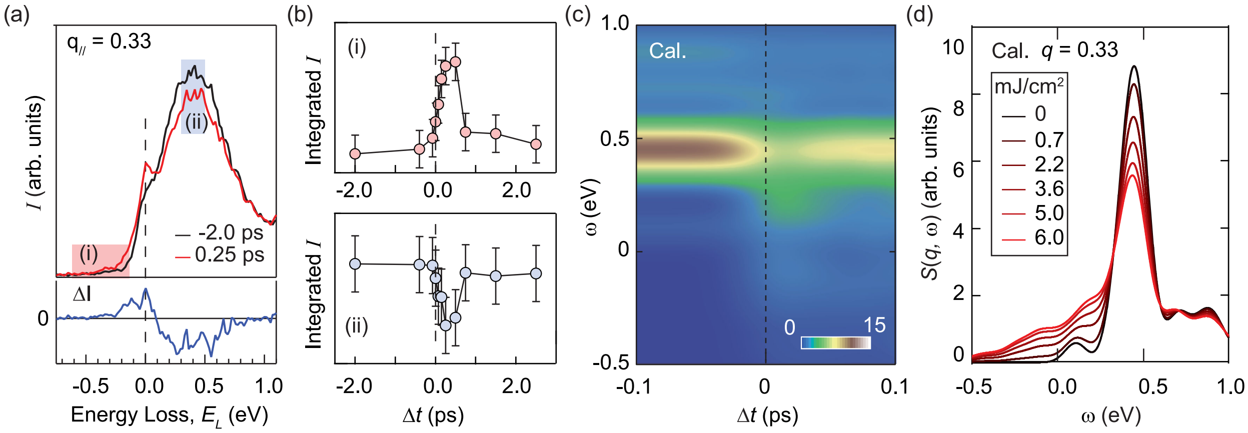

FIG. 3. (a) RIXS spectra at $q_{\parallel} = 0.33$ r.l.u. before and after time zero with the differential spectrum shown in the lower panel. (b) Time traces of the integrated intensity within windows (i) and (ii) indicated in panel (a). The error bars were estimated from the noise level of the RIXS spectrum. (c) Time dependence of calculated dynamical spin structure factor $S(q, \omega, t)$ at $\mathbf{q} = (0.33, 0)$ for 6 mJ/cm^2 pump, obtained using the single-band Hubbard model. (d) Fluence dependence of calculated $S(q, \omega, t)$ at the center of the pump ($\Delta t = 0$) for same momentum as panel (c).

reflect modifications in the spectral line shapes of paramagnons and plasmons across the Brillouin zone. As will be elaborated below, these spectral changes extend into the quasielastic region, giving rise to an apparent increase in the quasielastic peak intensity, highlighted in red. As a function of time, shown in Fig. 2(c) for a representative momentum $q_{\parallel} = -0.125$ r.l.u., the light-induced response exhibits a rapid onset and attains its maximum amplitude at approximately 0.1 ps. This characteristic timescale is comparable to the experimental temporal resolution of ~0.15 ps, indicating that the effect is predominantly generated during the pump pulse. Afterward, the light-induced changes diminish and have almost returned to their equilibrium form after 1.5 ps. While plasmons also show interesting variations, their three-dimensional nature requires out-of-plane momentum-dependent measurements for full characterization [29], which is beyond the scope of our data. Therefore, in this Letter, we focus only on the behavior of the paramagnons.

We first examine raw RIXS spectra taken at $q_{\parallel} = 0.33$ r.l.u., a momentum where only the paramagnon excitation is present. Upon pumping, as shown in Fig. 3(a), the paramagnon peak intensity is suppressed without changing the peak position. In addition, the spectral weight in the energy gain regime is increased at least up to $E_L =$ -0.3 eV, indicating the presence of anti-Stokes scattering from certain modes, whose population substantially increases due to the pump. The modes, whose energy scales significantly exceed the maximum phonon energy in cuprates (~80 meV), are most likely paramagnons, given that they are the dominant mode at this momentum with a matching energy scale. Because recovery of the magnetic degree of freedom requires dissipation of pump-induced paramagnons, the energy-gain spectral weight should follow the same temporal evolution as the paramagnon peak in the energy-loss channel. This is confirmed in Fig. 3(b): both the integrated energy-gain spectral weight [window (i)] and the paramagnon peak intensity [window (ii)] show nearly identical time dependence, supporting the assignment of the energy-gain features to a light-induced paramagnon population. We remark that due to the paramagnon's broad peak width (i.e., short lifetime), anti-Stokes scattering does not manifest as a distinct peak, but rather as additional spectral weight on the energy gain side (see Supplemental Material Fig. S2 [26]), as observed in our data. Also, in this situation, the spectral weight at zero energy becomes finite, resulting in an increase of the elastic peak intensity, as seen in our data (Figs. 2 and 3). We also acknowledge that multiphonon annihilation may occur and account for part of the anti-Stokes spectral weight, though it cannot be isolated in our current data. A quantitative assessment would require polarization-resolved RIXS measurements, which are not yet feasible with the present trRIXS setup at x-ray FEL facilities.

To address the observed light-driven paramagnon variation, we perform time-dependent exact diagonalization simulations for the time-resolved dynamical spin structure factor $S(\mathbf{q}, \omega, \Delta t)$, using the single-band Hubbard model on a 12-site cluster with 16.7% electron doping, which is the closest doping to that of our experimental sample that can be realized in this cluster (see Supplemental Material [26]). Pump photon energy and polarization are identical to those used in the experiment. Figures 3(c) and 3(d) present the $S(\mathbf{q}, \omega, \Delta t)$ calculated at its smallest accessible nonzero momentum $q_{\parallel} = 0.33$ r.l.u. for our cluster (see Supplemental Material Sec. G [26]). In equilibrium, before the pump pulse arrives, the spectrum exhibits a peak at 400 meV corresponding to the paramagnon excitation in NCCO. At the center of the pump ($\Delta t = 0$), this peak height decreases rapidly. At the same time, lower energy

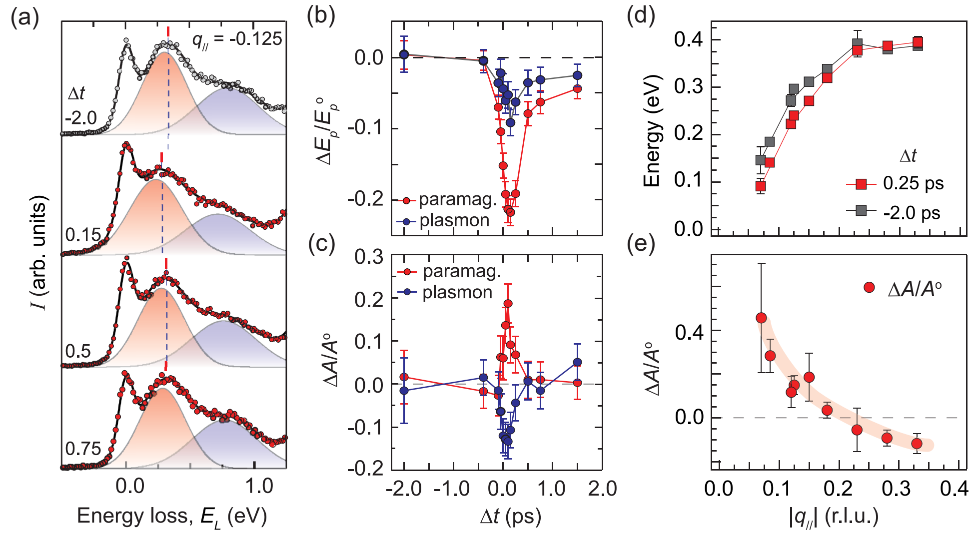

FIG. 4. (a) RIXS spectra at representative time delays at $q_\parallel = -0.125$ r.l.u.. The red ticks are the apparent paramagnon peak position in raw data the dashed lines are guide-of-the eye for the shift of the paramagnon peak position. The red and blue shaded peaks represent the fitted paramagnon and plasmon. (b) Time traces of normalized peak position changes for paramagnon and plasmon. (c) Time traces of normalized spectral weight changes for paramagnon and plasmon. (d) Summary of the fitted paramagnon positions E_p before (black markers) and after (red markers) time zero. (e) Momentum dependence of the normalized change of the paramagnon spectral weight (area of the fitted paramagnon) $\Delta A = A^{(0.25\ \mathrm{ps})} - A^o$, where $A^o = A^{(-2.0\ \mathrm{ps})}$. Shaded area are guide to the eye. The error bars were estimated via standard propagation of uncertainty from the 95% confidence level from the fit of the peak parameter.

spectral weight extending to the energy gain ($\omega < 0$) increases, manifest as the broadening of the paramagnon excitation. We also found that the main peak position is essentially unchanged [Fig. 3(c)] and not sensitive to the pump fluence [Fig. 3(d)], which primarily impacts spectral weight suppression and anti-Stokes spectral weight generation. The behavior of $S(\mathbf{q}, \omega, \Delta t)$ is consistent with our experimental observation at $q_\parallel = 0.33$ r.l.u.. We have also performed trRIXS calculations, which match the behaviors of the calculated $S(\mathbf{q}, \omega, \Delta t)$, ruling out potential artifacts stemming from the finite-core-hole life time and matrix element effects (Supplemental Material Fig. S3 [26]).

Moving toward the Brillouin zone center, the behavior of the paramagnons with small $q_\parallel$ appears to be more complex. As shown in Fig. 4(a), at $q_\parallel = -0.125$ r.l.u., while broadened, the paramagnon peak position in the raw spectra shifts to lower energy near time zero due to the pump. To disentangle it from the evolution of the plasmon in the same spectrum, we fitted the trRIXS spectra to extract the paramagnon peak as a function of Δt. Given that the paramagnon is overdamped and the evolution of its anti-Stokes and Stokes part are locked near time zero [Fig. 3(b)], we approximate the paramagnon spectrum with a single Gaussian peak spanning across zero energy, as superimposed in Fig. 4(a) (see also Supplemental Material and Fig. S4 [26]). As summarized in Fig. 4(b), the fitted paramagnon peak position softens by approximately 20%, accompanied by an increase of paramagnon spectral weight [Fig. 4(c)]. These behaviors are in contrast to the paramagnon at $q_\parallel = 0.33$ r.l.u., where the peak position remains unchanged and the spectral weight decreases.

Apparently, the light-driven paramagnon variation exhibits a momentum dependence within the Brillouin zone. Figure 4(d) shows the paramagnon dispersion along the h direction before and after time zero, obtained by fitted paramagnon peak positions as a function of $q_\parallel$ at $\Delta t = -2.0$ and 0.25 ps, respectively (see Supplemental Material Fig. S5 [26] for data and fitting). The paramagnon softening is most prominent near the zone center and diminishes when moving toward the zone boundary, resulting in a modulation of the paramagnon dispersion without changing the paramagnon bandwidth. Moreover, the light-induced change in paramagnon spectral weight is also momentum dependent, as shown in Fig. 4(e). For small momenta, the pump increases the spectral weight due to a significant portion of light-driven paramagnons in the energy gain via anti-Stokes scattering (see Supplemental Material Fig. S5 [26]). Interestingly, the enhancement in spectral weight rapidly decreases with increasing momentum and eventually changes sign near $q_\parallel \sim 0.2$ r.l.u., beyond which the overall spectral weight begins to decrease due to the pump. Altogether, our results, for the first time, demonstrate that the photoexcitation can modify the paramagnon dispersion and redistribute the spectral weight within the Brillouin zone.

We remark that the dispersion modification does not necessarily imply that the underlying spin exchange interaction is modulated by the pump. Particularly, in the small $q_\parallel$ regime where the energy scale is also smaller, the paramagon peak position softening can be due to the substantial anti-Stokes fraction in the overall paramagnon spectral weight (see also Supplemental Material Figs. S2 and S4 [26]). The fact that the paramagnon peak position essentially remains unchanged near the zone boundary (i.e., identical paramagnon dispersion bandwidth) thereby asserts no alteration in the spin-exchange coupling strength, at least along the h direction in our pump-probe geometry. We note that photoexcitation can create electron-hole pairs in the Cu $3d$ and O $2p$ states, which could, in principle, influence the AFM coupling. However, the spatial scale of pair production is set by the pump wavelength, and the number of such pairs is controlled by the pump excitation density. Given that the pump excitation density is substantially smaller than the limit of creating one pair per unit cell (see Supplemental Material [26] Sec. D), changes in the paramagnon peak position at large momentum, dominated by local spin exchange, would not be expected to be greatly affected by the presence of photoexcitated pairs.

To contextualize our findings, we correlate the observed paramagnon evolution with quasiparticle dynamics in the photoexcited state [7,28]. Near time zero, photoexcitation generates hot electrons that rapidly form a pseudo-Fermi distribution with an effective electronic temperature. In this period, the paramagnon population increases, their dispersion is modulated, and spectral weight is redistributed in the Brillouin zone. The initial relaxation of hot electrons occurs by transferring energy to strongly coupled phonons on a timescale of a few hundred femtoseconds, matching the initial paramagnon recovery observed in our data. Thus, after photoexcitation, hot-electron relaxation and restoration of magnetic degrees of freedom proceed in tandem. Beyond a few picoseconds, the electronic, magnetic, and lattice subsystems reach a quasiequilibrium and then recover more slowly. As a remark, while the phonon bath in this picture is generally accepted, a direct probe of the lattice is still lacking. Time-resolved x-ray diffraction would be ideal for this purpose but lies beyond the scope of this Letter.

In this context, a natural question is whether the light-induced paramagnon response can be described in terms of an effective "magnetic" temperature, similar to the typical description of quasiparticles. At elevated temperatures, the paramagnon population will be higher, which enhances the anti-Stokes spectral weight and broadens the paramagnon peak (Supplemental Material Fig. S6 [26]). Thus, the light-induced paramagnon peak broadening and the increase of anti-Stokes spectral weight appears to be attributable to an increased effect magnetic temperature. However, the altered dispersion at fixed bandwidth and the associated redistribution of total spectral weight do not fully align with the simple heating picture. Our determinant quantum Monte Carlo (DQMC) simulations based on canonical ensemble [33] show that, at high temperatures, the paramagnon energy at the zone boundary should also be reduced (see Supplemental Material Fig. S7 [26]), because thermally generated doublon-hole pairs, which move randomly in the copper-oxide plane, substantially lower the average energy required to flip a spin and decrease the spin correlation length. In contrast, in the photoexcited nonequilibrium state, the pump field can additionally drive mobile charge carriers through the antiferromagnetic background along the direction of the pump's electric field, thereby scrambling spin orientations and perturbing the magnetic subsystem in a manner that cannot be captured solely by an effective temperature increase.

Since the paramagnon spectral weight reflects its density of state, and thereby playing an important role in mediating electron-AFM coupling [34], any redistribution of the spectral weight in the Brillouin zone can transiently alter the character and strength of the coupling. Specifically, our observation of a reduced spectral weight at large $q_{\|}$ implies a weaker coupling between electrons and magnetic fluctuation at higher momentum, likely including those near the (π, π) point. Consequently, this diminished electron—AFM coupling may be a key factor contributing to the filling-in of the pseudogap at the Fermi-surface hot spots in photoexcited NCCO [25].

More broadly, the ultrafast modulation of dispersion and the generation of substantial populations of high-momentum magnetic modes offer a compelling pathway for magnonic devices [35], which require efficient magnon generation and transport. Given that prototypical materials for magnonic applications—such as yttrium iron garnet (YIG)—are characterized by robust long-range magnetic order and intrinsically low magnetic damping, we expect that optically generated magnons in these systems will exhibit substantially longer lifetimes than the paramagnons observed in optimally doped NCCO. In summary, our results reveal that photoexcitation can reshape collective magnetic behavior. Looking ahead, especially when paired with tailored pump pulses, ultrafast excitation offers powerful new leverage for actively controlling the magnetic properties of materials.

Acknowledgments—The experimental work was supported by the U.S. Department of Energy, Office of Basic Energy Sciences, Materials Sciences and Engineering Division under Contract No. DE-AC02-76SF00515. Theoretical simulations (J. H., S. D., and Y. W.) were supported by the U.S. Department of Energy, Office of Science, Basic Energy Sciences, under Early Career Award No. DE-SC0024524. We acknowledge European XFEL in Schenefeld, Germany, for provision of x-ray free-electron laser beamtime at SCS under Proposal No. 3078 and would like to thank the staff for their assistance. D. J. gratefully acknowledges funding by the Alexander-von-Humboldt foundation. The simulation used resources of the National Energy Research Scientific Computing Center, a U.S. Department of Energy Office of Science User Facility located at Lawrence Berkeley National Laboratory, operated under Contract No. DE-AC02-05CH11231. T. C. A. acknowledges funding from the Heisenberg resonant inelastic x-ray scattering (hRIXS) consortium. G. M. and G. G. acknowledge support by the Italian Ministry of University and Research (MUR) through the project FIS2 "abovEF" FIS-2023-02406.

Data availability—The data that support the findings of this article are publicly available at Zenodo [36].

[1] B. Keimer, S. A. Kivelson, M. R. Norman, S. Uchida, and J. Zaanen, From quantum matter to high-temperature superconductivity in copper oxides, Nature (London) **518**, 179 (2015).

[2] D. N. Basov, R. D. Averitt, and D. Hsieh, Towards properties on demand in quantum materials, Nat. Mater. **16**, 1077 (2017).

[3] Y. H. Wang, H. Steinberg, P. Jarillo-Herrero, and N. Gedik, Observation of Floquet-Bloch states on the surface of a topological insulator, Science **342**, 453 (2013).

[4] Y. Wang, M. Claassen, C. D. Pemmaraju, C. Jia, B. Moritz, and T. P. Devereaux, Theoretical understanding of photon spectroscopies in correlated materials in and out of equilibrium, Nat. Rev. Mater. **3**, 312 (2018).

[5] A. de la Torre, D. M. Kennes, M. Claassen, S. Gerber, J. W. McIver, and M. A. Sentef, Colloquium: Nonthermal pathways to ultrafast control in quantum materials, Rev. Mod. Phys. **93**, 041002 (2021).

[6] C. Giannetti, M. Capone, D. Fausti, M. Fabrizio, F. Parmigiani, and D. Mihailovic, Ultrafast optical spectroscopy of strongly correlated materials and high-temperature superconductors: A non-equilibrium approach, Adv. Phys. **65**, 58 (2016).

[7] M. Zonno, F. Boschini, and A. Damascelli, Time-resolved arpes on cuprates: Tracking the low-energy electrodynamics in the time domain, J. Electron Spectrosc. Relat. Phenom. **251**, 147091 (2021).

[8] R. Mankowsky, A. Subedi, M. Först, S. O. Mariager, M. Chollet, H. T. Lemke, J. S. Robinson, J. M. Glownia, M. P. Minitti, A. Frano, M. Fechner, N. A. Spaldin, T. Loew, B. Keimer, A. Georges, and A. Cavalleri, Nonlinear lattice dynamics as a basis for enhanced superconductivity in $YBa_2Cu_3O_{6.5}$, Nature (London) **516**, 71 (2014).

[9] M. Först, R. I. Tobey, H. Bromberger, S. B. Wilkins, V. Khanna, A. D. Caviglia, Y.-D. Chuang, W. S. Lee, W. F. Schlotter, J. J. Turner, M. P. Minitti, O. Krupin, Z. J. Xu, J. S. Wen, G. D. Gu, S. S. Dhesi, A. Cavalleri, and J. P. Hill, Melting of charge stripes in vibrationally driven $La_{1.875}Ba_{0.125}CuO_4$: Assessing the respective roles of electronic and lattice order in frustrated superconductors, Phys. Rev. Lett. **112**, 157002 (2014).

[10] M. Mitrano, S. Lee, A. A. Husain, L. Delacretaz, M. Zhu, G. de la Peña Munoz, S. X.-L. Sun, Y. I. Joe, A. H. Reid, S. F. Wandel, G. Coslovich, W. Schlotter, T. van Driel, J. Schneeloch, G. D. Gu, S. Hartnoll, N. Goldenfeld, and P. Abbamonte, Ultrafast time-resolved x-ray scattering reveals diffusive charge order dynamics in $La_{2-x}Ba_xCuO_4$, Sci. Adv. **5**, eaax3346 (2019).

[11] H. Jang *et al.*, Characterization of photoinduced normal state through charge density wave in superconducting $YBa_2Cu_3O_{6.67}$, Sci. Adv. **8**, eabk0832 (2022).

[12] S. Wandel *et al.*, Enhanced charge density wave coherence in a light-quenched, high-temperature superconductor, Science **376**, 860 (2022).

[13] D. Jost, E. G. Lomeli, T. Tang, J. J. Kas, J. J. Rehr, W.-S. Lee, H.-C. Jiang, B. Moritz, and T. P. Devereaux, Time-resolved x-ray spectroscopy from the atomic orbital ground state up, Phys. Rev. X **15**, 011012 (2025).

[14] M. Mitrano and Y. Wang, Probing light-driven quantum materials with ultrafast resonant inelastic x-ray scattering, Commun. Phys. **3**, 184 (2020).

[15] M. P. M. Dean *et al.*, Ultrafast energy- and momentum-resolved dynamics of magnetic correlations in the photo-doped Mott insulator Sr_2IrO_4, Nat. Mater. **15**, 601 (2016).

[16] D. G. Mazzone *et al.*, Laser-induced transient magnons in $Sr_3Ir_2O_7$ throughout the Brillouin zone, Proc. Natl. Acad. Sci. U.S.A. **118**, e2103696118 (2021).

[17] H. Lu, A. Gauthier, M. Hepting, A. S. Tremsin, A. H. Reid, P. S. Kirchmann, Z. X. Shen, T. P. Devereaux, Y. C. Shao, X. Feng, G. Coslovich, Z. Hussain, G. L. Dakovski, Y. D. Chuang, and W. S. Lee, Time-resolved RIXS experiment with pulse-by-pulse parallel readout data collection using x-ray free electron laser, Sci. Rep. **10**, 22226 (2020).

[18] E. Paris, C. W. Nicholson, S. Johnston, Y. Tseng, M. Rumo, G. Coslovich, S. Zohar, M. F. Lin, V. N. Strocov, R. Saint-Martin, A. Revcolevschi, A. Kemper, W. Schlotter, G. L. Dakovski, C. Monney, and T. Schmitt, Probing the interplay between lattice dynamics and short-range magnetic correlations in $CuGeO_3$ with femtosecond RIXS, npj Quantum Mater. **6**, 51 (2021).

[19] J. Schlappa *et al.*, The Heisenberg-RIXS instrument at the European XFEL, J. Synchrotron Radiat. **32**, 29 (2025).

[20] E. M. Motoyama, G. Yu, I. M. Vishik, O. P. Vajk, P. K. Mang, and M. Greven, Spin correlations in the electron-doped high-transition-temperature superconductor $Nd_{2-x}Ce_xCuO_{4+\delta}$, Nature (London) **445**, 186 (2007).

[21] R. L. Greene, P. R. Mandal, N. R. Poniatowski, and T. Sarkar, The strange metal state of the electron-doped cuprates, Annu. Rev. Condens. Matter Phys. **11**, 213 (2020).

[22] N. P. Armitage, P. Fournier, and R. L. Greene, Progress and perspectives on electron-doped cuprates, Rev. Mod. Phys. **82**, 2421 (2010).

[23] K.-J. Xu, J. He, S.-D. Chen, Y. He, S. N. Abadi, C. R. Rotundu, Y. S. Lee, D.-H. Lu, Q. Guo, O. Tjernberg, T. P. Devereaux, D.-H. Lee, M. Hashimoto, and Z.-X. Shen, Anomalous normal-state gap in an electron-doped cuprate, Science **385**, 796 (2024).

[24] J. He, C. R. Rotundu, M. S. Scheurer, Y. He, M. Hashimoto, K.-J. Xu, Y. Wang, E. W. Huang, T. Jia, S. Chen, B. Moritz, D. Lu, Y. S. Lee, T. P. Devereaux, and Z. xun Shen, Fermi surface reconstruction in electron-doped cuprates without antiferromagnetic long-range order, Proc. Natl. Acad. Sci. U.S.A. **116**, 3449 (2019).

[25] F. Boschini, M. Zonno, E. Razzoli, R. P. Day, M. Michiardi, B. Zwartsenberg, P. Nigge, M. Schneider, E. H. da Silva

Neto, A. Erb, S. Zhdanovich, A. K. Mills, G. Levy, C. Giannetti, D. J. Jones, and A. Damascelli, Emergence of pseudogap from short-range spin-correlations in electron-doped cuprates, npj Quantum Mater. **5**, 6 (2020).

[26] See Supplemental Material at http://link.aps.org/supplemental/10.1103/2h9x-8tjk for additional details.

[27] Y. Onose, Y. Taguchi, K. Ishizaka, and Y. Tokura, Charge dynamics in underdoped $Nd_{2-x}Ce_xCuO_4$: Pseudogap and related phenomena, Phys. Rev. B **69**, 024504 (2004).

[28] L. Perfetti, P. A. Loukakos, M. Lisowski, U. Bovensiepen, H. Eisaki, and M. Wolf, Ultrafast electron relaxation in superconducting $Bi_2Sr_2CaCu_2O_{8+\delta}$ by time-resolved photoelectron spectroscopy, Phys. Rev. Lett. **99**, 197001 (2007).

[29] M. Hepting *et al.*, Three-dimensional collective charge excitations in electron-doped copper oxide superconductors, Nature (London) **563**, 374 (2018).

[30] J. Lin, J. Yuan, K. Jin, Z. Yin, G. Li, K.-J. Zhou, X. Lu, M. Dantz, T. Schmitt, H. Ding, H. Guo, M. P. M. Dean, and X. Liu, Doping evolution of the charge excitations and electron correlations in electron-doped superconducting $La_{2--x}Ce_xCuO_4$, npj Quantum Mater. **5**, 4 (2020).

[31] W. S. Lee *et al.*, Asymmetry of collective excitations in electron- and hole-doped cuprate superconductors, Nat. Phys. **10**, 883 (2014).

[32] K. Ishii, M. Fujita, T. Sasaki, M. Minola, G. Dellea, C. Mazzoli, K. Kummer, G. Ghiringhelli, L. Braicovich, T. Tohyama, K. Tsutsumi, K. Sato, R. Kajimoto, K. Ikeuchi, K. Yamada, M. Yoshida, M. Kurooka, and J. Mizuki, High-energy spin and charge excitations in electron-doped copper oxide superconductors, Nat. Commun. **5**, 3714 (2014).

[33] S. Ding, S. Li, and Y. Wang, Sampling electronic Fock states using determinant quantum Monte Carlo, Commun. Phys. **8**, 48 (2025).

[34] M. Le Tacon *et al.*, Intense paramagnon excitations in a large family of high-temperature superconductors, Nat. Phys. **7**, 725 (2011).

[35] A. V. Chumak, V. I. Vasyuchka, A. A. Serga, and B. Hillebrands, Magnon spintronics, Nat. Phys. **11**, 453 (2015).

[36] W. S. Lee, Data for the paper, entitled "Collective Magnetic Excitations in a Photo-excited Electron-doped Cuprate Superconductor" [Dataset] (2026), 10.5281/zenodo.21365825.